ARTICLE NO. 79-0145R

C80-028

High-Speed Interference Heating Loads and Pressure Distributions Resulting from Elevon Deflections

20003
20007
20017

Charles B. Johnson*
NASA Langley Research Center, Hampton, Va.
and
Louis G. Kaufman II†
Grumman Aerospace Corporation, Bethpage, N.Y.

Effects of elevon-induced three-dimensional shock wave turbulent boundary-layer interactions on hypersonic aircraft surfaces are analyzed. Detailed surface pressure and heating rate distributions obtained on wing-elevon-fuselage models representative of aft portions of hypersonic aircraft are compared with analytical and experimental results from other sources. Examples are presented that may be used to evaluate the adequacy of current theoretical methods for estimating the effects of three-dimensional shock wave turbulent boundary-layer interactions on hypersonic aircraft surfaces.

Nomenclature

H = ratio of disturbed to undisturbed heat transfer coefficients at same location
h = heat transfer coefficient, W/m^2K
M = Mach number
P = pressure ratio, (P/P_∞) disturbed/(P/P_∞) undisturbed
p = pressure, Pa
R_c = Reynolds number based on freestream flow conditions and length (64.14 cm wing root chord)
t = time, s
T = temperature, K
x = streamwise distance measured along surface of wing and elevon from wing apex (wing leading edge for unswept wing), cm
y = spanwise distance measured outboard from inboard edge of the elevon, cm
z = distance measured on end plate surface upward from wing surface, cm
ϵ = elevon deflection angle, deg
θ = elevon shock wave angle, deg
Λ = wing sweepback angle, deg

Subscripts

aw = adiabatic wall
i = initial
inv = value calculated inviscidly, neglecting separation
pc = phase change of paint coating
PK = peak (maximum conditions)
t = stagnation conditions of freestream tunnel flow
l = local flow conditions over wing and over wing and end plate surfaces
∞ = freestream flow conditions

Presented as Paper 79-0145 at the 17th Aerospace Sciences Meeting, New Orleans, La., Jan. 15-17, 1979; submitted March 2, 1979; revision received Sept. 7, 1979.

Index categories: Boundary Layers and Convective Heat Transfer—Turbulent; Supersonic and Hypersonic Flow; Jets, Wakes, and Viscid-Inviscid Flow Interactions.

*Aerospace Engineer, Subsonic-Transonic Aerodynamics Division. Member AIAA.

†Senior Staff Scientist, Research Department. Associate Fellow AIAA.

Introduction

COMPONENTS of hypersonic aircraft are subjected to severe pressure and thermal loads. For the most part, these loads can be estimated using scale model experimental results and analytical methods. However, existing methods are not adequate for estimating the loads on portions of the aircraft where there are strong shock wave boundary-layer interactions. The problem is particularly complex for three-dimensional flow interactions.

For example, deflecting a flap or elevon causes a shock wave in the inviscid flow over the aircraft surface. The shock wave interacts with the viscid boundary layer flow on the surface and frequently causes flow separation, which changes: 1) the effective shape of the surface, 2) the external flow, and 3) the distribution and magnitude of pressure and thermal loads on the surface. The control effectiveness can be greatly reduced below the value calculated by inviscid fluid flow analyses, and the loads induced on adjacent surfaces can extend over much larger regions than anticipated using inviscid flow analyses, thus requiring more extensive heat shielding.

Inviscid-viscid interaction flow problems generally have eluded theoretical solutions because of their complexity. Aspects of some purely two-dimensional, and of some simple three-dimensional, interaction flows can now be predicted fairly reliably using empirically verified methods,[1-3] but cannot be predicted adequately for general three-dimensional interaction flows.[1,4,5] This work was conducted to improve the understanding of three-dimensional shock wave boundary-layer interaction flows and to provide data useful for determining the accuracy of current analytic methods for predicting pressure and thermal loads in interaction flow regions.

Experimental Program

Model Design Criteria

Instead of testing a complete aircraft configuration, a "half" model representative of the aft portion of winged hypersonic aircraft was used in order to obtain realistic wing-root-chord Reynolds number data in existing wind tunnel facilities.[6] Using half-wing models such as those shown in Figs. 1 and 2, more detailed information could be obtained in the three-dimensional interaction flow region and the wing-root-chord Reynolds number could be made comparable to those anticipated for flight configurations. The character of the boundary layer, which is very important in interaction

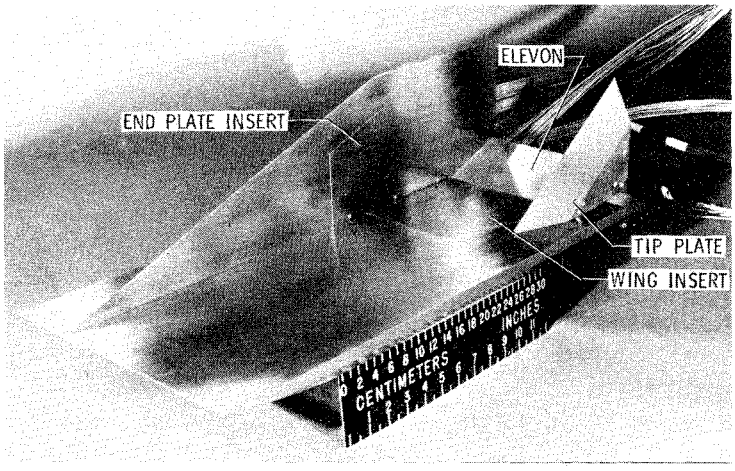

Fig. 1 Photograph of wing elevon pressure model; $\Lambda = 0$ deg, $\epsilon = 30$ deg.

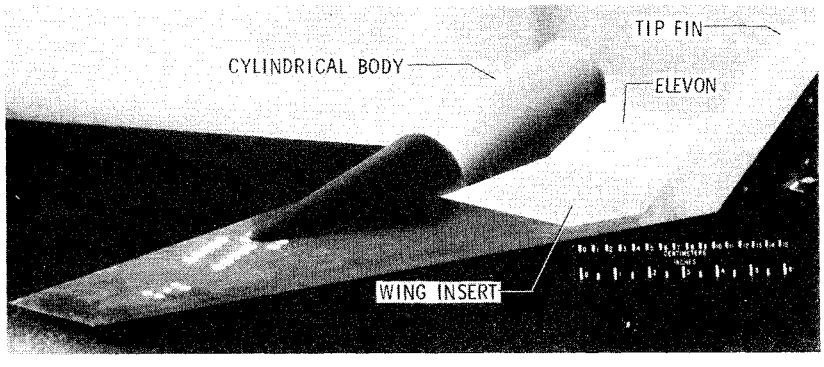

Fig. 2 Photograph of wing elevon heat transfer model; $\Lambda = 70$ deg, $\epsilon = 20$ deg.

flow regions,[7] therefore more closely approximates that for full-scale flight vehicles. This is particularly important ahead of trailing edge controls on swept wings where the boundary layer may be characteristically turbulent inboard and laminar outboard.[8]

Model Description

Unswept, 50 deg swept, and 70 deg swept half wings with machined sharp leading edges were fabricated. The wings had replaceable trailing edge elevons with chord lengths of 8.89 cm and 13.97 cm (14 and 22% of wing root chord, respectively) that could be set at (flow compression) deflection angles ranging from 0 to 30 deg in 5 deg increments. Flat plate (end plate, see Fig. 1) and cylindrical center bodies (Fig. 2) were attachable to the wings, as well as several tip fins.[6]

The wings, elevons, and end plate had replaceable inserts used to obtain either surface pressure distributions (Fig. 1) or heat transfer rate coefficient distributions (Fig. 2). (The cylindrical center body was used only for surface heating rate distributions.) Stainless steel inserts with pressure orifices and tubes were used for the pressure data tunnel runs. These were replaced by silicone rubber inserts for the heat transfer data runs. The silicone rubber inserts (0.64 cm thick) were well suited for obtaining heat transfer data using the phase change paint technique.[9] The inserts—in the tip fins, end plate, cylindrical body, wings, and elevons—encompassed the interaction flow region.

Tunnel and Test Conditions

The Langley 20-inch Mach 6 Tunnel used for these experiments is a blowdown wind tunnel with a fast operating model injection system located beneath the test section. Nominal values of stagnation pressure and temperature for the Mach 6 Tunnel flow were: $p_t = 3.56 \times 10^6$ N/m^2 (516 psia) and $T_t = 520$ K (940°R). The resulting freestream Reynolds number, based upon the wing-root-chord length of 64.14 cm, is: $R_c = 18.5 \times 10^6$.

Data Reduction

The measured model surface pressures were nondimensionalized using the freestream static pressure for each tunnel run. The resulting pressure ratios, p/p_∞, are insensitive to minor variations in the tunnel flow pressure from run to run.

Surface distributions of aerodynamic heat transfer coefficients were obtained using the phase change paint technique described by Jones and Hunt.[9] When injected into the tunnel flow and subjected to aerodynamic heating, the paint melts on the model surfaces (first in the regions of highest heating), and the progression of the paint melt line on the model surfaces with time is recorded using motion picture cameras. The local heat transfer coefficient h at the melt line is calculated using the transient one-dimensional heat conduction equation in the form:

$$h\sqrt{t_{pc}}/\sqrt{\rho ck} = f(T_{pc} - T_i / T_{aw} - T_i)$$

where ρck are thermophysical properties of the silicone rubber.[6] The universal, transcendental function f, of the phase change, initial and adiabatic wall temperatures, has been plotted by Jones and Hunt. The adiabatic wall temperature values used in the equation for these test results were calculated for a turbulent boundary-layer recovery factor of 0.896.

Experimental Results

Detailed surface pressure and aerodynamic heating rate coefficient distributions coupled with profile Schlieren photographs (Fig. 3) and surface oil film flow pictures (Fig. 4) were obtained to delineate regions of interacting flow on the model surfaces.[6] Schlieren photographs (Fig. 3) were used to define the change in curvature of the shock wave emanating from the elevon hinge line: from convex at low elevon angles to concave at large elevon angles. This information was used

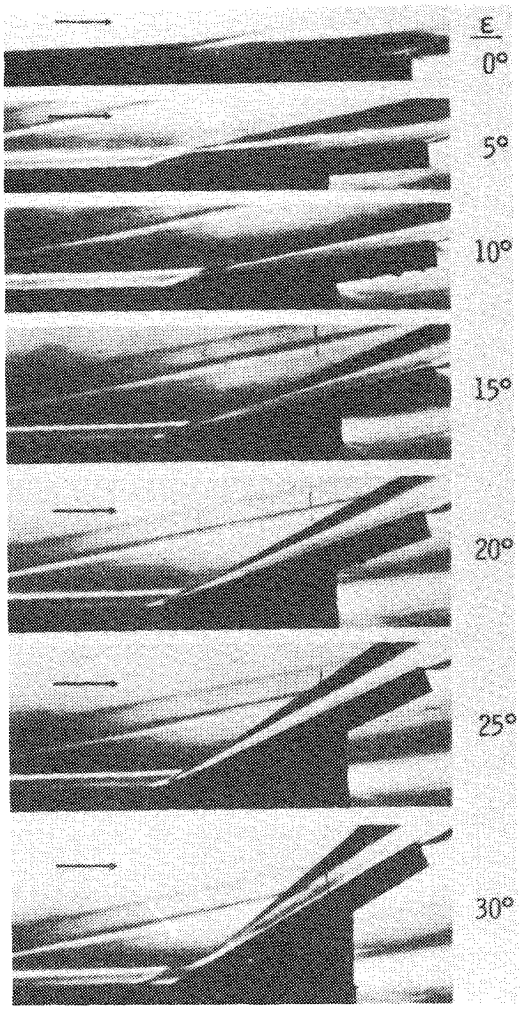

Fig. 3 Schlieren flow photographs for elevon deflections; $\Lambda = 0$ deg, $M_\infty = 6$.

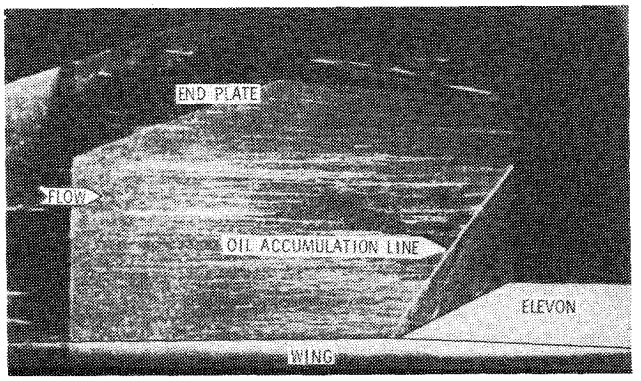

Fig. 4 Oil flow picture showing oil accumulation line on end plate; $\Lambda = 0$ deg; $\epsilon = 20$ deg.

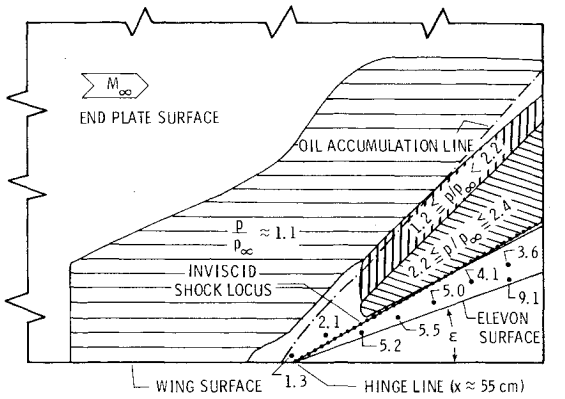

Fig. 5 Pressure distribution (p/p_∞) on end plate surface; $\Lambda = 0$ deg; $\epsilon = 20$ deg.

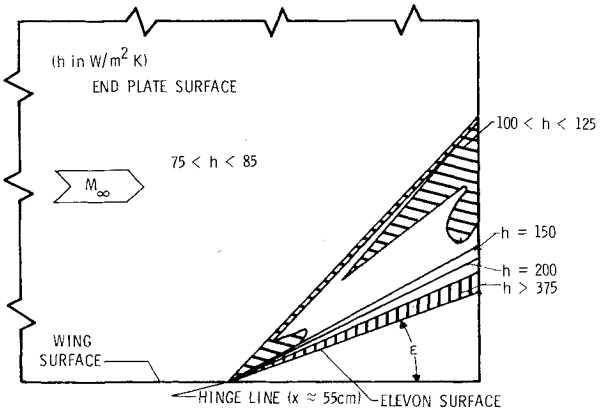

Fig. 6 Regions of interference heating on end plate; $\Lambda = 0$ deg; $\epsilon = 20$ deg.

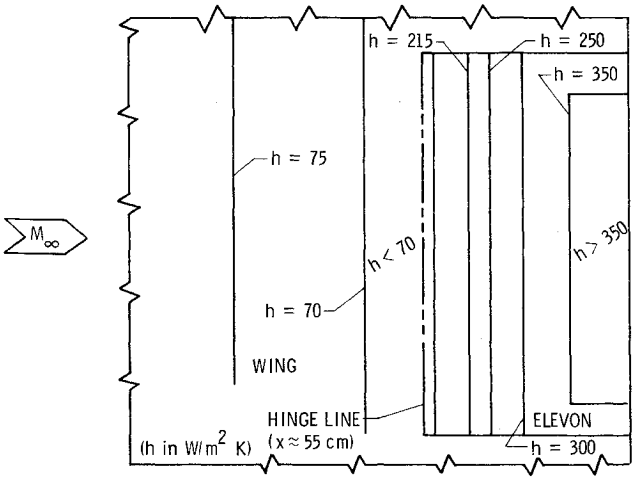

Fig. 7 Constant h contours on wing and elevon; $\Lambda = 0$ deg; $\epsilon = 20$ deg.

in analyzing the two-dimensional flow field over the wing and elevon.

Oil film photographs of the end plate surface (ϵ = 20 deg, e.g., Fig. 4), indicate a much larger region of disturbed flow than would be anticipated using two-dimensional inviscid flow analyses.[5] The location of the oil accumulation line on the end plate shown in Fig. 5 delineates the region of increased pressure on the end plate surface. The locus of the elevon-induced inviscid two-dimensional shock wave on the end plate surface is also shown in Fig. 5. A comparison of Figs. 4 and 5 indicates that the surface oil flow on the end plate follows the decreasing pressure gradient with a flow almost normal to the elevon surface in the region of high pressure. In the regions of lower pressure, the surface flow bends downstream, moving almost parallel to the oil accumulation line in the outer extent of the iteration region.

Regions and contours of heating are indicated by the heat transfer rate coefficient h and are shown in Figs. 6 and 7 (for ϵ = 20 deg) on the end plate, wing, and elevon surfaces for the same model configuration. The region of increased heating on the end plate surface is demarcated quite well by the oil film accumulation line[5] and the boundaries of the heating regions essentially follow the regions of pressure (compare Figs. 4, 5, and 6). There is no evidence of flow separation on the wing or

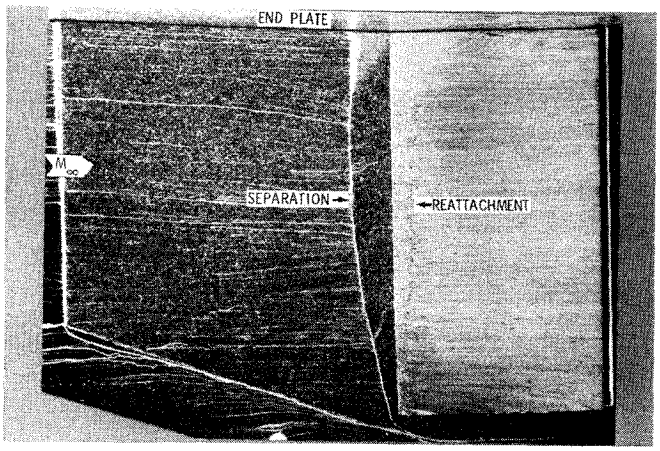

Fig. 8 Oil flow picture showing wing and elevon surfaces, with end plate attached; $\Lambda = 70$ deg; $\epsilon = 30$ deg.

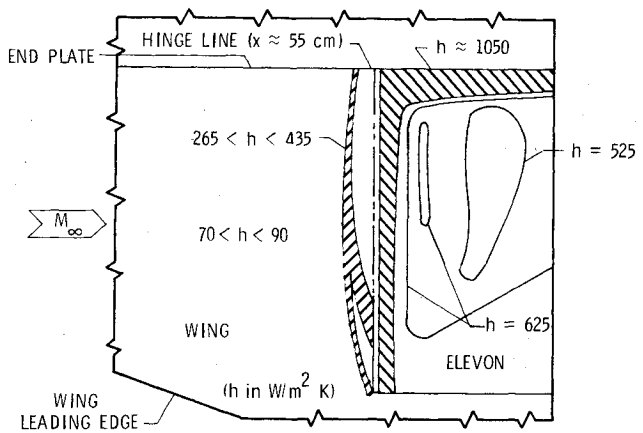

Fig. 9 Regions of interference heating on wing and elevon surfaces, with end plate attached; $\Lambda = 70$ deg; $\epsilon = 30$ deg.

elevon based on Schlieren photographs, oil flow studies, and pressure distributions,[6] and also the absences of increased heating just upstream of the hinge line for the 20 deg elevon (Fig. 7).

The 30 deg elevon, however, induces turbulent boundary-layer separation from the wing surface upstream of the hinge line.[6] The region of separated flow is delineated by the oil accumulation line in Fig. 8 and matches the region of increased heating on the wing surface indicated by the cross-hatched region of heating ($265 < h < 435$) in the upstream portion of the separated region shown in Fig. 9. The highest heating on the elevon is associated with the reattachment region just downstream of the hinge line and the interaction region near the intersection of the elevon and the end plate. The maximum extent of turbulent boundary-layer separation ahead of the midspan of the 30 deg elevon is fairly constant with or without the end plate attached to the wing.[6] With the end plate the separated region on the inboard portion of the wing and elevon (adjacent to the end plate) does not close into the hinge line as it does in the outboard portion of the elevon (see Figs. 8 and 9), thus indicating the three-dimensional nature of the flow in the separated region.

When the end plate is replaced by the cylindrical center body, the separated flow region ahead of the 30 deg elevon becomes more complex and highly three-dimensional (Fig. 10). The maximum extent for separated flow is nearly twice that with either no center body or with the end plate attached to the wing.[6] The heat transfer coefficient ranges 200-350 W/m^2K in the upstream portion of the separated region on the wing as shown in Fig. 11. This region of increased heating resembles the region delineated by the oil accumulation line

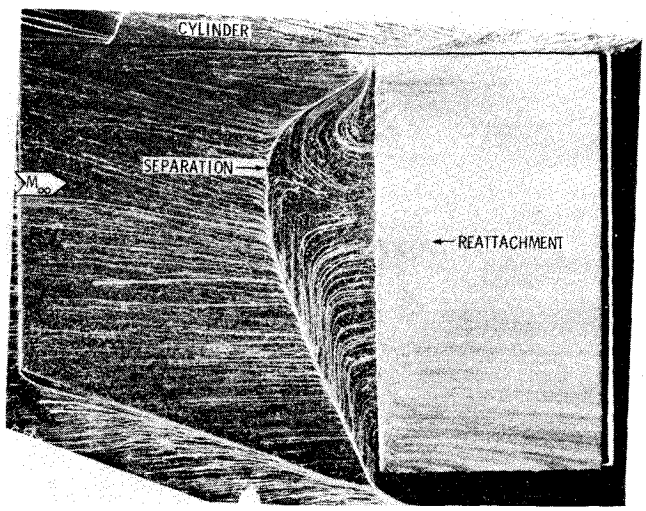

Fig. 10 Oil flow picture showing wing and elevon, with cylindrical body attached; $\Lambda = 70$ deg; $\epsilon = 30$ deg.

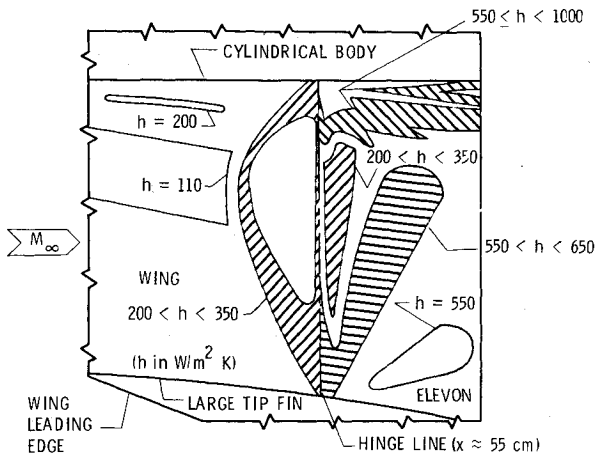

Fig. 11 Regions of interference heating on wing and elevon surfaces, with cylindrical body and tip fin attached; $\Lambda = 70$ deg; $\epsilon = 30$ deg.

for the same configuration (compare Figs. 10 and 11). The highest heating ($500 < h < 1000$, Fig. 11) occurs on the elevon in the region next to the cylindrical body where the shock around the 80 deg swept body interacts with compression shock over the elevon and produces streaks of high interference heating. As expected, there is also high heating ($500 < h < 650$) in the region of reattachment on the elevon. The effect of the shock from the cylindrical body can also be seen on the heating on the wing as indicated by the $h = 200$ region. The large change in the location of the oil accumulation line on the wing surface ahead of the 30 deg elevon, when the end plate is replaced by the cylindrical center body, is indicated in Fig. 12. However, streamwise tip fins and end plates have relatively little effect on the separated flow region. As shown in Fig. 13, there is only a small change in the separation line shape and location when the end plate and tip plate are attached to the model with a 30 deg deflected elevon.

Results and Comparisons

Streamwise pressure distributions along the elevon midspan line are compared with pressure rises calculated using two-dimensional, inviscid flow theory in Fig. 14 for the unswept configuration with no inboard or outboard attachments. Although there are methods that more accurately predict two-dimensional pressure rises in the presence of strong viscid effects, even these more precise methods are inadequate for predicting either the extent or magnitude of the increased

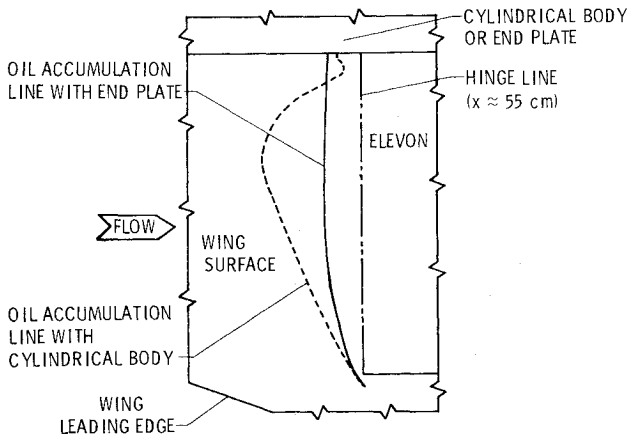

Fig. 12 Oil accumulation lines ahead of elevon with two side shapes; $\Lambda = 70$ deg; $\epsilon = 30$ deg.

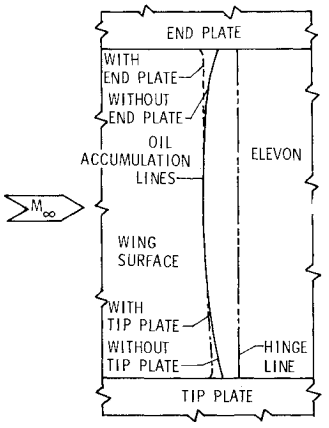

Fig. 13 End plate and tip plate effects on oil accumulation lines upstream of elevon; $\Lambda = 0$ deg; $\epsilon = 30$ deg.

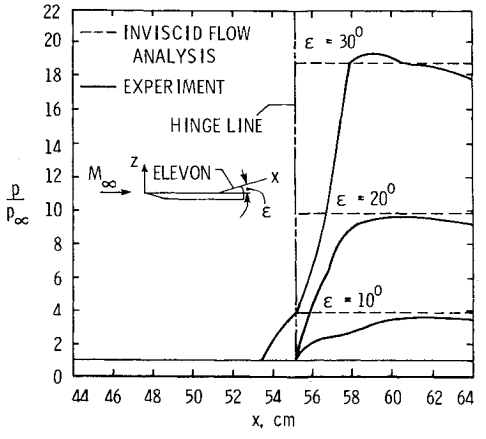

Fig. 14 Pressure distributions on wing and along elevon mid-span line; $\Lambda = 0$ deg.

pressure loads in general three-dimensional shock wave boundary-layer interaction regions.[10]

Similarly, heat transfer rate coefficient distributions along the elevon midspan line are plotted in Fig. 15 for both the 9 cm and 14 cm long elevons. These data are compared with a theoretical distribution calculated from an integral method which used the measured pressure distribution, coupled with the Van Driest II skin friction theory, a modified form of the Reynolds analogy, and the assumption of a virtual origin at the hinge line.[6,11] There are significant differences between the measured and calculated values in the upstream portion of

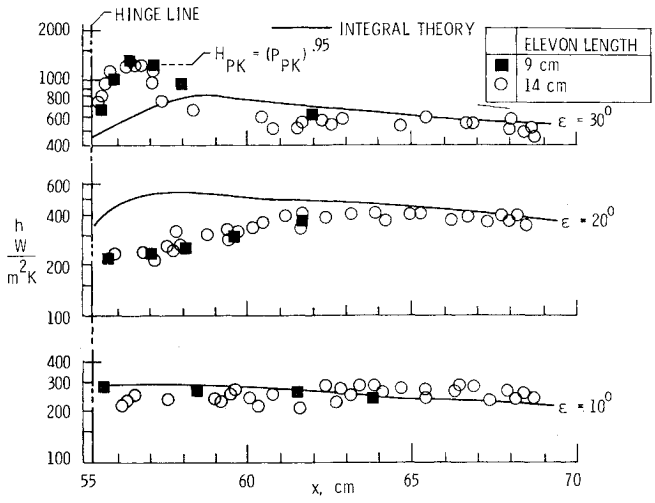

Fig. 15 Elevon heating along mid-span line; $\Lambda = 0$ deg.

the elevon, particularly for the $\epsilon = 20$ deg and 30 elevons; however, in all cases the experimental distributions approach the theory in the downstream portion of the 14 cm long elevon.

Both the magnitude and location of high heating rate coefficients are strongly dependent upon specific vehicle geometry, such as wing sweep, center body configuration (i.e., end plate or cylindrical body), as well as other effects which would not be anticipated using current analyses. Even for these comparatively simple geometries, the heating rate distributions depend strongly upon the particular geometry.[6]

Pressure rises on the end plate surface, induced by 20 and 30 deg elevons, are shown in Fig: 16 and are compared with two-dimensional, inviscid flow calculations. Although the region of increased pressure induced on the end plate is much larger, the total side force induced on the end plate is somewhat less (85 to 98%) than that calculated using two-dimensional inviscid fluid flow analyses.[6] Wing sweep and the addition of tip fins have little effect on the force induced on the end plate.

Scuderi,[3] Hayes,[12] and others proposed analytical methods for estimating pressure and heating rate distribution for planar three-dimensional interaction flow regions. These analytical methods are based on observations of experimental results and correlations of empirical data from many sources. The interaction region studied by Scuderi and Hayes consists of a shock wave generated by a sharp leading edge, unswept fin interacting with a turbulent boundary layer on the flat plate surface on which the fin is mounted. Except for the boundary layer on the surface upstream of the elevon, their geometry is similar to that discussed herein, with the fin simulating the elevon and the flat plate simulating the end plate. Sample comparison of these two theories with the current experimental data for a 20 deg elevon are shown in Figs. 17 and 18. The data and analytical results were compared at a point near the trailing edge of the elevon (7.6 cm). At the 7.6 cm station, the distance from the hinge line is relatively large compared to the boundary-layer thickness at the same station on the end plate, which is one of the requirements of the analytical methods. The peak and plateau pressures correlate well with $M_l \sin\theta$, and the location of the peak pressure occurs along rays that correlate with $(\theta - \epsilon)$. The location of the outward extent of the interaction region is asymptotic to a ray from a virtual origin located upstream of the hinge line.

The peak and plateau pressures predicted by the theory of Scuderi are higher than the data (Fig. 17). The prediction by the methods of Hayes is slightly higher for the peak pressure, but shows good agreement in the plateau region. Both theories predict the extent of the interaction. The prediction of heating

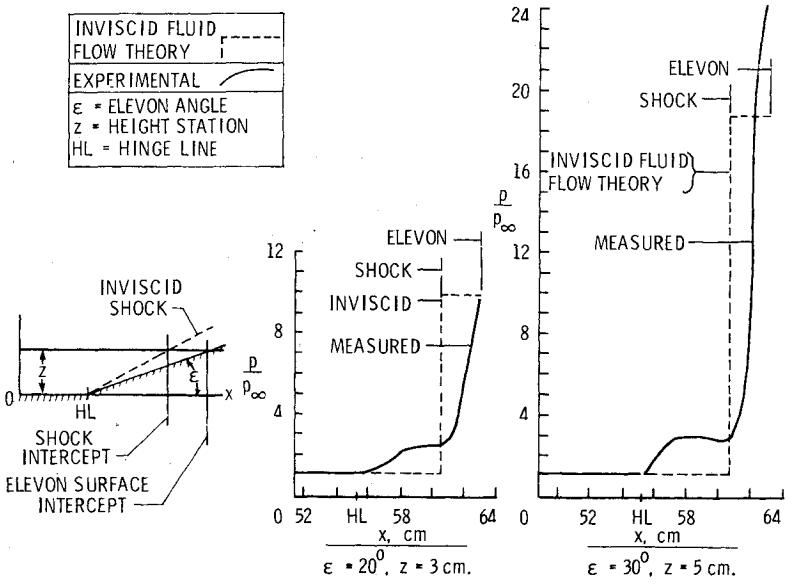

Fig. 16 Pressure distributions on the end plate for two elevon deflections; $\Lambda = 0$ deg.

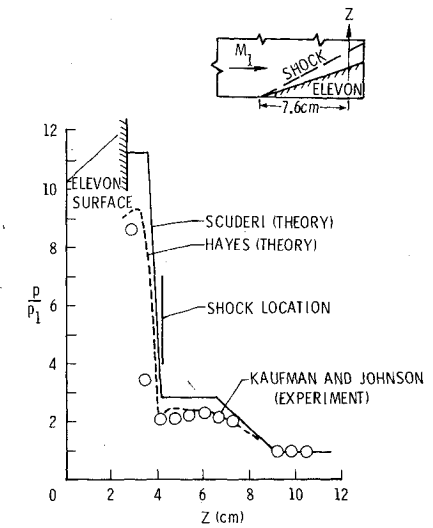

Fig. 17 Comparison of data and theory for pressures on the end plate; $\Lambda = 0$ deg, $\epsilon = 20$ deg.

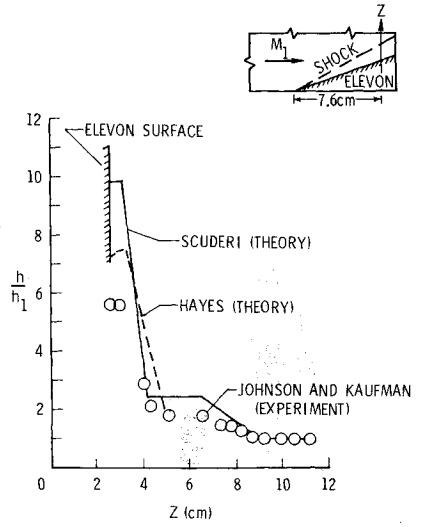

Fig. 18 Comparison of data and theory for heating rates on the end plate; $\Lambda = 0$ deg, $\epsilon = 20$ deg.

in Fig. 17 is higher than the data for both theories. The difference between data and theory in Figs. 17 and 18 may be a result of the thicker boundary-layer over the elevon than over the fin used in the analytical models. The increase in the heating rates are considerably larger than for two-dimensional separated flows.[12] These sample methods may be used to predict accurately some facets of planar three-dimensional interaction flows, but are not adequate for general three-dimensional interaction flows. For instance, the methods are not applicable directly when separation occurs upstream of the hinge line, and are not applicable to non-planar center bodies.

Conclusion

Detailed surface pressure and aerodynamic heating rate distributions were obtained on several fundamental configurations[6] to serve as a guide in estimating increased pressure and thermal loads caused by elevon deflections on hypersonic aircraft. Existing analytical methods predict some facets of three-dimensional interaction flows for simple configurations composed of purely planar surfaces, but are inadequate for general three-dimensional configurations.

Some specific conclusions, based upon experimental results and observations, are:

Pressure and heating rate distributions on swept wing surfaces are unaffected by 10 and 20 deg elevon deflections for turbulent boundary layer flow. Pressures and heating rates on the wing surfaces are increased in the separated turbulent boundary-layer flow region ahead of 30 deg elevons. An inboard (planar) end plate and wing tip fin have relatively little effect on the separated flow region, except that they tend to make it more nearly two-dimensional. The cylindrical body, however, strongly affects the separated flow region, making it more extensive and highly asymmetric.

The elevons induce increased pressures and heating rates on the adjacent end plate and cylindrical body surfaces over regions that are much more extensive than would be anticipated using inviscid flow analyses. However, the total side force induced on the end plate is less than anticipated.

References

[1] Korkegi, R.H., "Survey of Viscous Interactions Associated with High Mach Number Flight," *AIAA Journal*, Vol. 9, May 1971, pp. 771-783.

[2] Johnson, C.B. and Kaufman, L.G. II, "Incident Shock Interactions with Boundary Layers," *Journal of Spacecraft and Rockets*, Vol. 12, June 1975, pp. 327-329.

[3] Scuderi, L.F., "Expressions for Predicting 3-D Shock Wave—Turbulent Boundary Layer Interaction Pressures and Heating Rates," AIAA Paper No. 78-162, Jan. 1978.

[4] Edwards, A.J., "Heat Transfer Distributions on a 70° Delta Wing with Flap-Induced Separation," Imperial College Aero Report 75-01, March 1975.

[5] Goldberg, T.J., "Three-Dimensional Separation for Interaction of Shock Waves with Turbulent Boundary Layers," *AIAA Journal*, Vol. 11, Nov. 1973, pp. 1573-1575.

[6] Kaufman, L.G. II and Johnson, C.B., "Pressure and Thermal Loads Induced by Elevon Deflections on Swept Wings and Adjacent Surfaces at Mach 6," NASA TP-1356, 1979.

[7] Chapman, D.R., Kuehn, D.M., and Larson, H.K., "Investigation of Separated Flows in Supersonic and Subsonic Streams with Emphasis on the Effect of Transition," NACA Report 1356, 1958.

[8] Kaufman, L.G. II and Freeman, L.M., "Separation Ahead of Controls on Swept Wings," Aerospace Research Laboratories TR 75-0134, U.S. Air Force, June 1975.

[9] Jones, R.A. and Hunt, J.L., "Use of Fusible Temperature Indicators for Obtaining Quantitative Aerodynamic Heat-Transfer Data," NASA TR R-230, 1966.

[10] Hankey, W.L. Jr. and Holden, M.S., "Two-Dimensional Shock Wave Boundary Layer Interactions in High Speed Flows," AGARDograph 203, NATO, June 1975.

[11] Johnson, C.B. and Boney, L.R., "A Simple Integral Method for the Calculation of Real-Gas Turbulent Boundary Layers with Variable Edge Entropy," NASA TN D-6217, June 1971.

[12] Hayes, J.R., "Prediction Technique for the Characteristics of Fin Generated Three-Dimensional Shock Wave Turbulent Boundary Layer Interactions," AFFDL TR 77-10, U.S. Air Force, May 1977.